Acta Pharmaceutica Sinica B 2021;11(12):3935–3949

Chinese Pharmaceutical Association
Institute of Materia Medica, Chinese Academy of Medical Sciences

Acta Pharmaceutica Sinica B

www.elsevier.com/locate/apsb
www.sciencedirect.com

ORIGINAL ARTICLE

DNA-PK inhibition by M3814 enhances chemosensitivity in non-small cell lung cancer

Manni Wang[†], **Siyuan Chen**[†], **Yuquan Wei, Xiawei Wei***

Laboratory of Aging Research and Cancer Drug Target, State Key Laboratory of Biotherapy and Cancer Center, National Clinical Research Center for Geriatrics, West China Hospital, Sichuan University, Chengdu 610000, China

Received 22 April 2021; received in revised form 21 June 2021; accepted 9 July 2021

KEY WORDS

M3814;
Paclitaxel;
Etoposide;
DNA-dependent protein kinase;
Non-small cell lung cancer;
DNA repair;
Cell senescence;
Chemosensitization

Abstract A significant proportion of non-small cell lung cancer (NSCLC) patients experience accumulating chemotherapy-related adverse events, motivating the design of chemosensitizating strategies. The main cytotoxic damage induced by chemotherapeutic agents is DNA double-strand breaks (DSB). It is thus conceivable that DNA-dependent protein kinase (DNA-PK) inhibitors which attenuate DNA repair would enhance the anti-tumor effect of chemotherapy. The present study aims to systematically evaluate the efficacy and safety of a novel DNA-PK inhibitor M3814 in synergy with chemotherapies on NSCLC. We identified increased expression of DNA-PK in human NSCLC tissues which was associated with poor prognosis. M3814 potentiated the anti-tumor effect of paclitaxel and etoposide in A549, H460 and H1703 NSCLC cell lines. In the four combinations based on two NSCLC xenograft models and two chemotherapy, we also observed tumor regression at tolerated doses *in vivo*. Moreover, we identified a P53-dependent accelerated senescence response by M3814 following treatment with paclitaxel/etoposide. The present study provides a theoretical basis for the use of M3814 in combination with paclitaxel and etoposide in clinical practice, with hope to aid the optimization of NSCLC treatment.

Abbreviations: DDR, DNA damage response; DNA-PK, DNA-dependent protein kinase; DNA-PKcs, DNA-dependent protein kinase catalytic subunit; DSB, DNA double-strand breaks; dsDNA, double strand DNA; HR, homologous recombination; IHC, immunohistochemistry; LADC, lung adenocarcinoma; LCLC, large-cell carcinoma; LSCC, lung squamous cell carcinoma; NHEJ, non homologous end joining; NSCLC, non-small cell lung cancer.

*Corresponding author.
E-mail address: xiaweiwei@scu.edu.cn (Xiawei Wei).
[†]These authors made equal contributions to this work.

Peer review under responsibility of Chinese Pharmaceutical Association and Institute of Materia Medica, Chinese Academy of Medical Sciences.

https://doi.org/10.1016/j.apsb.2021.07.029

1. Introduction

Non-small cell lung cancer (NSCLC) is a worldwide malignancy and the leading cause of cancer-related mortality[1]. Surgical resection remains the primary treatment for NSCLC at early stage[2]. On one hand, a large proportion of patients are diagnosed at advanced stage and are thus ineligible for operations[3]. On the other hand, only a small number of patients benefit from the postoperative adjuvant chemotherapy[4].

DNA double-strand breaks (DSBs) are considered as the most lethal form of cytotoxic damage[5−7]. DSB can be caused by endogenous or exogenous toxins, and if left unrepaired, can lead to cell cycle arrest and cell deaths. The potent DNA damage repair system in tumor cells includes non homologous end joining (NHEJ) and homologous recombination (HR) pathway, contributing to the therapeutic resistance of tumor cells[8]. HR repair pathway is mostly active during S phase, whereas NHEJ pathway can occur in all cell cycle phases, suggesting that HR mainly repairs DSBs that occur during DNA replication[9]. It also has to be addressed that the DNA repair kinetics of NHEJ pathway is faster than that of HR pathway[10,11]. NHEJ is thus characterized as the major DSB repair pathway in mammalian cells.

Previous reports have emphasized DNA-dependent protein kinase (DNA-PK) as an essential component of the NHEJ pathway[12]. DNA-PK is a serine/threonine protein kinase consisting of the catalytic subunit of DNA-PK (DNA-PKcs), and a heterodimer composed of the Ku70 and Ku80 subunits[13]. In the light of the crucial function of DNA-PK in DNA damage response (DDR), DNA-PK targeted therapy potentially works in synergy with DNA-damaging agents[14]. Once DSBs are induced, the Ku70/80 heterodimers rapidly recognize and flock to the DNA damage sites[15−17], and form a cyclic structure which stabilizes the broken ends of double strand DNA (dsDNA). Furthermore, Ku heterodimers recruit DNA-PKcs to form a synaptic complex at the DNA termini which holds the broken ends of dsDNA together[18−21]. The binding of DNA-PKcs to the DSB sites then leads to the translocation of the Ku70/80 and the subsequent activation of DNA-PKcs[22,23].

Substantial literature has identified relatively higher expression of DNA-PK in cancer tissues. For example, compared with adjacent normal mucosa, esophageal cancer tissues exhibit increased DNA-PK expression by 49%. The death risk of NSCLC patients with high DNA-PKcs expression is 2.13 times higher than that with normal expression[24]. On the other hand, the expression of DNA-PK in tumor cells is significantly correlated with tumor response to DNA-damaging agents[25]. In the residual cervical cancer cells that were resistant to radiotherapy, the expression of DNA-PKcs was markedly elevated, indicating a positive correlation between radiation resistance and DNA-PK expression levels[26]. Likewise, the down-regulation of DNA-PKcs was correlated with the increased radiosensitivity of lymphoblastic cell lines[27], whereas the increased DNA-PKcs expression limited the response to standard radiotherapy in prostate cancer patients[28].

Based on these findings, it is conceivable that the inhibition of DNA-PK is an attractive strategy to overcome resistance to DSB-inducing treatments in cancer cells. Old-generation DNA-PK inhibitors have been proved effective but are limited in terms of selectivity due to structural similarities with PI3Ks[29]. M3814 represents the new-generation of selective DNA-PK protein kinase inhibitors[30]. Recent preclinical studies mainly focused on M3814 activity in combination with chemotherapies in ovarian cancer[31] and acute myeloid leukemia (AML)[32], or with ionizing radiation in lung cancer[33]. The aim of the present study is to evaluate the efficacy and safety of M3814 in synergy with paclitaxel and etoposide to treat NSCLC, and to explore the possible mechanism of action, so as to provide theoretical basis for the use of M3814 in combination with paclitaxel and etoposide in clinical practice.

2. Materials and methods

2.1. Patient cohorts and tissue specimens

Tumor specimens and clinical data of patients were provided by Shanghai Outdo Biotech (National Engineering Centre for Biochip at Shanghai, China). The informed consent was obtained from patients and the study was approved by the Ethics Committee of National Human Genetic Resources Sharing Service Platform (permit number: 2005DKA21300). Tumor tissues and their adjacent normal tissue specimens were obtained from 174 patients diagnosed with non-small cell lung cancer who underwent surgical resections between July 2004 and June 2006. The median survival time was defined as the time duration between initial diagnosis of NSCLC to the final follow-up visit. Tissue specimens were immersed in 4% paraformaldehyde, embedded in paraffin, and then stained with anti-DNA-PKcs antibody (CST, #12311S). The paraffin-embedded tissues were independently graded by two board-certified pathologists. Based on the percentage of cells positive for DNA-PKcs nuclear staining in the whole field, the positive staining rate of tissues were scored as follows: 0 (negative), 1 (1%−25%), 2 (26%−50%), 3 (51%−75%), 4 (76%−100%), whereas the staining intensity was scored as: 0 (negative), 1 (weak), 2 (medium), and 3 (strong). Final expression scores were recorded as positive staining rates × staining intensity.

2.2. Reagents and antibodies

M3814 was purchased from Medchemexpress (MCE, HY-101570). Paclitaxel and etoposide phosphate were purchased form Selleck Chemicals (S1150) and Meilunbio (MB1102), respectively. For *in vitro* studies, M3814 and etoposide was initially dissolved in dimethyl sulfoxide (DMSO; Sigma) as 100 mmol/L stock solution and stored at −20 °C. The stock solution was diluted to reach corresponding concentrations and added to cell cultures. Treatment controls were set as the 0.5% DMSO, the same volume as the other groups. For *in vivo* experiments, M3814 were orderly added with the following solvent: 10% DMSO, 40% PEG400 (Sigma−Aldrich), 5% Tween-80 (Sigma−Aldrich) and 45% saline. Anti-phospho-histone γ-H2AX (Ser139) was purchased from Abcam (ab11174; Cambridge, UK). Anti-P53 antibody was purchased from HUABIO (ET1601-13; Hangzhou, China). Anti-P21 (2947S), anti-DNA-PKcs (12311S) and anti-p-DNA-PK (Ser2056, 68716S) antibodies were purchased from Cell Signaling Technology (CST, MA, USA). Anti-GAPDH antibody was purchased from Santa Cruz Biotechnology (sc-32233; Santa Cruz, CA, USA). Fluorescent secondary antibodies were obtained from Invitrogen.

2.3. Cell lines and culture

The human NSCLC cell lines A549, H460 and H1703 were provided by the American Type Culture Collection (ATCC, Rockville, MD, USA). Cell lines were cultured in RPMI 1640

containing 10% fetal bovine serum (FBS; Gibco) and 1% antibiotics (penicillin and streptomycin, Gibco) at 37 °C with 5% CO_2.

2.4. Cell viability assay

Cell viability of NSCLC cell lines treated with either M3814 alone, or in combination with etoposide was evaluated by the Counting Kit-8 (CCK-8) provided by MCE, according to the kit instructions. In brief, 100 μL of A549 and H460 cells were seeded in 96-well plates (1000−4000 cells/well) and pre-incubated for 24 h in a humidified incubator at 37 °C, 5% CO_2. Cells were treated with paclitaxel and etoposide (concentration gradient from 1 nmol/L to 100 μmol/L), in the absence or presence of M3814 (5 μmol/L). After incubation for an appropriate length of time (24, 48 and 72 h), 10 μL of CCK-8 solution and 90 μL fresh medium were added to each well and followed by 1−4 h of incubation at 37 °C. The absorbance of plates was measured at 450 nm using a microplate reader, and the half inhibitory concentration (IC_{50}) was calculated using Prism 7 (GraphPad software). The combination index (CI) of M3814 and chemotherapy was calculated with CalculSyn software using Chou Talalay method. Among them, synergistic effect is CI $<$ 1, cumulative effect is CI $=$ 1, antagonistic effect is CI $>$ 1[34].

2.5. Colony formation assays

A549 and H460 cells were treated with paclitaxel and etoposide in the absence or in the presence of M3814 (5 μmol/L) for 24 h, and then cultured in 6-well plates for another 14 days. Rinse wells with PBS for 3 times and stain cell colonies with crystal violet 0.5% solution for 10 min. After air drying at room temperature, plates were photographed under light microscopy for analyzing the number of colonies.

2.6. EdU-based proliferation assay

EdU (5-ethynyl-2′-deoxyuridine) is a thymine nucleoside analogue which can be inserted into replicating DNA when tumor cells proliferate, thus directly reflecting DNA replication activity. Click-iT EdU Assay Kit (RiBo Bio, Guangzhou, China) was used to label proliferating human NSCLC cells following the manufacturer's recommendation. In brief, A549 and H460 cells were seeded in 96-well plates overnight, and treated with paclitaxel (5 nmol/L) and etoposide (100 nmol/L) with or without M3814 (5 μmol/L) for 18 h. We next added EdU solutions to the plates and incubated for 2−3 h in the dark at 37 °C to enable the incorporation of EdU into the DNA. We then washed the plates and observed cells under the inverted fluorescent microscope (Carl Zeiss, Germany). EdU-positive cells (3 random fields at 10 ×) were quantified using ImageJ software. The EdU flow cytometry assay was performed according to manufacturer's instructions.

2.7. Cell apoptosis assays by flow cytometry

A549 and H460 cells were seeded in 6-well plates at 1×10^5 per well. Paclitaxel (5 nmol/L) and etoposide (100 nmol/L) with or without M3814 (5 μmol/L) was added to each well. The DMSO-treated group was used as the control. After incubation for 48 h, the cells were performed with Annexin V-FITC apoptosis detection kit. Briefly, the cells were harvested and washed twice with cold PBS and then resuspended. Each sample was stained with 5 μL of Annexin V-FITC for 10 min and subsequently stained with 5 μL of PI for 5 min in the dark at room temperature. All samples were acquired by flow cytometry (ACEA NovoCyte) and analysed with NovoExpress software. The Annexin V-FITC/PI apoptosis detection kit (556,547) was purchased from BD Biosciences (Oxford, UK).

2.8. Cell apoptosis assay by TUNEL staining

Grow A549 and H460 cells on 96-well plates and incubate cells with paclitaxel (5 nmol/L), etoposide (100 nmol/L) with or without M3814 (5 μmol/L) for 48 h, wash the slides twice with PBS and process directly according to manufacturer's instructions (Promega corporation G3250). Briefly, permeabilize cells by immersing the slides in 0.2% Triton® X-100 solution for 5 min, and equilibrate at room temperature for 5−10 min. Add 50 μL of rTdT incubation buffer to the cells on a 5 cm^2 area. Cell nuclei were stained with DAPI to assess gross cell morphology. Immediately analyze TUNEL fluorescence under a fluorescence microscope using fluorescein at 520 nm and DAPI at 460 nm.

2.9. Cell cycle analyses by flow cytometry

Exponentially growing A549 and H460 cells were seeded in 6-well plates and grown for 24 h. Cells were treated with 5 μmol/L M3814, 5 nmol/L paclitaxel, 100 nmol/L etoposide, or their combinations, and incubated for 12 h. Cells were then washed twice with PBS solution, fixed with 75% pre-cooling ethanol, and placed at −20 °C for at least 24 h. Wash and resuspend cells with PBS and incubate cells with 20 μL 1 mg/mL RNase A (Beyotime) for 30 min at 37 °C. Stain cells with 25 μg/mL propidium iodide (Sigma−Aldrich) for 30 min at room temperature. The cell cycle distribution was measured with flow cytometry (ACEA NovoCyte) and analyzed with NovoExpress software.

2.10. γ-H2AX focus assay by immunofluorescence

Cellular DSBs were quantified by the detection of γ-H2AX (Ser139) focus formation. A549 and H460 cells were grown on round 24 mm climbing sheets in 6-well plates and incubated in the presence or absence of 5 μmol/L M3814 for 1 h before adding 100 nmol/L paclitaxel or 1 μmol/L etoposide. Following extensive washing in drug-free medium, cells were incubated with or without 5 μmol/L M3814 for another 4 h, and then fixed in 4% paraformaldehyde, permeabilized in 0.5% Triton X-100, and blocked with 5% bovine serum albumin. Next, cells were incubated with anti-γ-H2AX (Ser139) antibodies overnight at 4 °C, washed with PBS and incubated with fluorescent secondary antibodies for 1 h at 37 °C away from light. Cell nuclei were stained with DAPI to assess gross cell morphology. The percentage of γ-H2AX (Ser139) (red) was determined at each time point, with data presented as mean ± standard deviation (SD).

2.11. Western blot analysis

After indicated treatment for designed time duration, cells were harvested and washed twice with cold PBS and lysed through RIPA Lysis Buffer (Beyotime) mixed with 1 × Protease Inhibitor Cocktail (Millipore). Cells then underwent grinding 30−60 s (Homogenizer, Servicebio KZ-II), and the supernatant was collected after centrifugation. With the use of the Pierce™ Rapid Gold BCA Protein Assay Kit (23,225; Thermo Fisher, USA), the protein quantification assay was performed to determine the

protein concentration for each cell lysate. Next, the cell lysates were mix with loading buffer (Beyotime) and denatured in 100 °C metal bath for 10 min. Equal amounts of protein and molecular weight marker were loaded into the proper of sodium dodecyl sulphate-polyacrylamide gel electrophoresis (SDS-PAGE) gels of appropriate concentration, and transferred onto polyvinylidene difluoride (PVDF) membranes. Next we blocked the membrane for 1 h at room temperature with 5% milk dissolved in Tris-buffered saline and 0.1% Tween-20 (TBS-T) followed by incubation with corresponding primary antibodies overnight at 4 °C. Membranes were washed 3 times with TBS-T, and incubated with secondary antibodies for 1 h at room temperature. Band images were acquired using darkroom development techniques for chemiluminescence (Bio-Rad Laboratories).

2.12. *Senescence-associated β-galactosidase assay*

Senescence β-Galactosidase Staining Kit was purchased from Cell Signaling Technology (9860S) and staining was performed according to manufacturer's guide. In brief, cells were treated with paclitaxel (5 nmol/L), etoposide (100 nmol/L) with or without M3814 (5 μmol/L) for 24 h and then incubated for another 72 h. Cells were then washed with PBS and fixed in fixative solution to for 10−15 min at room temperature. Next, we added β-galactosidase staining solution to plates and incubated the plates at 37 °C overnight in a non-CO_2, dry incubator. Images were obtained with a Leica inverted microscope at 200 × magnification.

2.13. *Gene silencing by P53-targeting siRNA*

The control double-stranded small RNA siRNA-Control and siRNA-P53 were designed and chemically synthesized based on sequences shown in Table 1 (GeneChem, Shanghai, China). Control scrambled siRNA had no bio-informatically predicted sequence target in the human genome and was used as a negative control. Lipofectamine™ 3000 Transfection Reagent (Thermo Fisher Scientific, Waltham, MA, USA) and Opti-MEM I (Thermo Fisher Scientific, Waltham, MA, USA) were used to perform the transfection, according to the manufacturer's protocol. Cells were incubated for 48 h in a 5% CO_2 incubator at 37 °C and then lysed for Western blot assays to examine the knockdown effect of siRNA.

2.14. *In vivo anti-tumor efficacy study*

Animal studies were conducted under Institutional Animal Care and Use Committee of Sichuan University approved guidelines for animal welfare. Human NSCLC cell lines A549 cells (1×10^7 cells/100 μL) and H460 cells (5×10^6 cells/100 μL) were subcutaneously injected into the right posterior flanks of female NOD-SCID (nod-obese diabetic/severe combined immunodeficient) mice (6 weeks old). When NSCLC xenografts s.c. reached 5 mm in diameter (7 days after implantation, $n = 7$ per group), mice were treated with 1) solvent (control); 2) single agent M3814 (50 mg/kg) i.g. daily; 3) paclitaxel (10 mg/kg) i.v. once 3 days; 4) etoposide (10 mg/kg) i.p. once 3 days; 5) M3814+paclitaxel combination; 6) M3814+etoposide combination. For combination treatment group, M3814 was given immediately before chemotherapy. M3814 and paclitaxel were dissolved in each solvent one by one: 10% DMSO, 40% PEG400, 5% Tween-80 and 45% saline, and etoposide was dissolved in 10% DMSO and 90% saline. Tumor volume was measured with two-dimensional electronic caliper and calculated as Eq. (1):

$$\text{Tumor volume} = a^2 \times b/2 \quad (1)$$

where a is the smallest diameter measurement, and b is the diameter largest measurement. Data were presented as median relative tumor volume (RTV), which was calculated as tumor volume divided by tumor volume on the initial day of treatment (Day 0).

2.15. *Statistical analysis*

Data were presented as mean ± SD of three separated experiments. We analyzed data with GraphPad Prism 7.0. The significance of differences between two groups were determined by Student's t test (parametric) and ANOVA multiple comparison tests. The expression of DNA-PKcs between NSCLC tissues and paired non-cancerous tissues was determined by χ^2 test. Statistically significant P values were labelled as: $^{*}P < 0.05$, $^{**}P < 0.01$, $^{***}P < 0.001$, $^{****}P < 0.0001$. Kaplan−Meier survival analyses and log-rank tests were performed to evaluate the correlation between clinicopathological characteristics and patient prognosis.

3. Results

3.1. *Expression of DNA-PKcs is upregulated in human NSCLC tissues and correlates with poor prognosis*

Clinicopathological characteristics of 174 NSCLC patients, including 91 with lung adenocarcinoma (LADC), 78 with lung squamous cell carcinoma (LSCC) and 5 with large-cell carcinoma (LCLC), are presented in Table 2. Among all patients, 10 patients with lung adenocarcinoma were excluded from assessment of DNA-PKcs expression, due to lack of paired adjacent noncancerous tissues. The five LCLC patients were excluded from survival analyses due to small sample size. Finally, DNA-PKcs expression levels of a total number of 164 human NSCLC tissues (81 LADC, 78 LSCC, and 5 LCLC) and their paired adjacent noncancerous tissues were detection of by immunohistochemistry (IHC) assays. The calculated IHC scores revealed an elevated expression level of DNA-PKcs in 164 paraffin-embedded NSCLC

Table 1 siRNAs used for *P53* knockdown.

Gene target	Sequence	
	Sense (5′−3′)	Antisense (5′−3′)
Negative control	UUCUCCGAACGUGUCACGUTT	ACGUGACACGUUCGGAGAATT
TP53-Homo-136	CCCGGACGAUAUUGAACAATT	UUGUUCAAUAUCGUCCGGGTT
TP53-Homo-846	GCACAGAGGAAGAGAAUCUTT	AGAUUCUCUUCCUCUGUGCTT
TP53-Homo-687	CCACCAUCCACUACAACUATT	UAGUUGUAGUGGAUGGUGGTT

Table 2 Clinicopathological information of NSCLC patients.

Variable	*n* (%)
Gender	
Male	130 (74.7)
Female	44 (25.3)
Tumor size	
$<$ 5 cm	119 (68.4)
$\geq$ 5 cm	55 (31.6)
Grade	
I	4 (2.3)
II	120 (69.0)
III	50 (28.7)
Histologic type	
Adenocarcinoma	91 (52.3)
Squamous cell carcinoma	78 (44.8)
Large cell lung carcinoma	5 (2.9)
T stage	
1	29 (16.7)
2	101 (58.0)
3	35 (20.1)
4	9 (5.2)
N stage	
x	22 (12.6)
0	92 (52.9)
1	32 (18.4)
2	24 (13.8)
3	4 (2.3)
M stage	
0	172 (98.9)
1	2 (1.1)
Tumor stage	
I–II	99 (56.9)
III–IV	75 (43.1)
DNA-Pkcs expression	
High	71 (40.8)
Low	103 (59.2)

tissue samples compared with their adjacent noncancerous tissues (Fig. 1A and B). DNA-PKcs expressions were divided as high and low according to the optimal cut-off values calculated from ROC analyses (Fig. 1C). Based on follow-up outcomes between November 2005 and August 2018, we further assessed the correlation between tumor DNA-PKcs levels and patient prognoses. The overall survival (OS) time of patients with low and high DNA-PKcs expression was 54.00 $\pm$ 27.69 and 38.5 $\pm$ 25.74 months, respectively. Kaplan–Meier analyses demonstrated that higher expression of DNA-PKcs was significantly associated with poorer OS in LADC patients (Fig. 1D, log-rank test, $\chi^2 = 5.53$, $P = 0.019$). Similar trends were observed in patients with LSCC, where patients with higher DNA-PKcs tumor expression presented shorter survival time (Fig. 1E, log-rank test, $\chi^2 = 10.76$, $P = 0.001$).

3.2. *M3814 potentiates the inhibitory effect of chemotherapy on NSCLC cell proliferation in vitro*

Initial experiments sought to determine the cytotoxic effects of chemotherapy alone (0–100 mmol/L), and in combination with DNA-PK inhibitor M3814 in NSCLC cell lines. Following 24, 48 and 72 h of treatment, cell viability was assessed with CCK-8 cytotoxicity assays. Both paclitaxel and etoposide exhibited a more potent inhibitory effect on cell proliferation when combined with 5 μmol/L M3814 (Supporting Information Fig. S1). The IC_{50} values of paclitaxel on A549 cells when used alone at 24, 48 and 72 h were 645.5, 386.1, and 11.14 nmol/L, respectively. With concomitant exposure to 5 μmol/L M3814, the IC_{50} of paclitaxel decreased to 6.19, 0.24 and 0.15 nmol/L respectively at 24, 48 and 72 h (Fig. S1). In H460 cell line, the IC_{50} of paclitaxel were 1.40 μmol/L, 15.15 nmol/L and 0.85 nmol/L, at 24, 48 and 72 h, which decreased to 2.88, 0.27 and 0.004 nmol/L, respectively, when combined with M3814 (Fig. S1). In H1703 cell line, the IC_{50} of paclitaxel were 1.80 μmol/L, 0.98 nmol/L and 0.42 nmol/L, at 24, 48 and 72 h, which decreased to 2.16, 0.14 and 0.01 nmol/L, respectively, when combined with M3814 (Fig. S1). Similar trends could be observed in cells treated with etoposide suggesting the chemo-sensitization effect of M3814 on NSCLC cells. Moreover, the inhibition on cell proliferation was dose- and time-dependent, with maximal inhibition observed in cells treated with 100 μmol/L of paclitaxel/etoposide for 72 h. To determine whether the enhancement of cell death induced by M3814–etoposide combination was synergistic, additive, or antagonistic, cells were treated with chemotherapy, M3814 or their combination for 48 h (Fig. 2A). The calculated CI values indicated that M3814 acted in a synergistic manner with paclitaxel/etoposide on A549 and H460 NSCLC cells (CI $<$ 1), and with etoposide at doses higher than 1 μmol/L on H1703 cells (Fig. 2A).

We next performed EdU–DNA incorporation assays to investigate the inhibitory effect of M3814 and etoposide on newly synthesized DNA. As shown in Fig. 2B, A549, H460 and H1703 cells undergoing 18 h of combinational treatment displayed a significant decrease in nuclear EdU fluorescence staining (green), compared with cells treated with monotherapy. The reduced nuclear incorporation of EdU was further verified by flow cytometry assays (Fig. 2C and D), with EdU-positive A549 cell counts decreased from 19.8 $\pm$ 0.49% to 5.67 $\pm$ 0.31% when M3814 was added to paclitaxel treatment, and 38.21 $\pm$ 0.89% to 3.96 $\pm$ 0.39% when added to etoposide. Similar trends were observed in H460 and H1703 cell lines. These results suggest the synergistic inhibition on cell proliferation by M3814–paclitaxel/etoposide combination through the impairment of DNA synthesis. Colony formation tests further demonstrated the chemo-sensitization effect of M3814 on NSCLC cells, as evidenced by the decrease of colonies formed by cells treated with combination therapy. While paclitaxel/etoposide monotherapy modestly reduced colony formation, the addition of M3814 markedly enhanced the inhibitory effect of chemotherapy on NSCLC cell lines (Fig. 2E and F).

3.3. *M3814 promotes cell apoptosis and G2/M cell cycle arrest induced by chemotherapy in vitro*

To elucidate potential mechanisms underlying chemo-potentiation by M3814 on cell death, NSCLC cells labelled with Annexin V/PI were analyzed by FACS. As shown in Fig. 3A and B, either etoposide or M3814 alone induced limited cell apoptosis following 48 h of indicated treatments. Moreover, the most prominent increase in cell apoptotic fractions was observed in the etoposide + M3814 combinational treatment group (26.40 $\pm$ 1.29% in A549, 29.54 $\pm$ 2.09% in H460, and 12.34 $\pm$ 1.94% in H1703), and paclitaxel + M3814 group (17.36 $\pm$ 0.73% in A549, 23.23 $\pm$ 0.37% in H460, and 33.59 $\pm$ 3.64% in H1703) as compared with etoposide (1.06 $\pm$ 0.24% in A549, 1.42 $\pm$ 0.38% in H460, and 4.52 $\pm$ 0.86% in H1703) and paclitaxel monotherapy group (7.52 $\pm$ 1.17% in A549, 4.53 $\pm$ 0.51% in H460, and

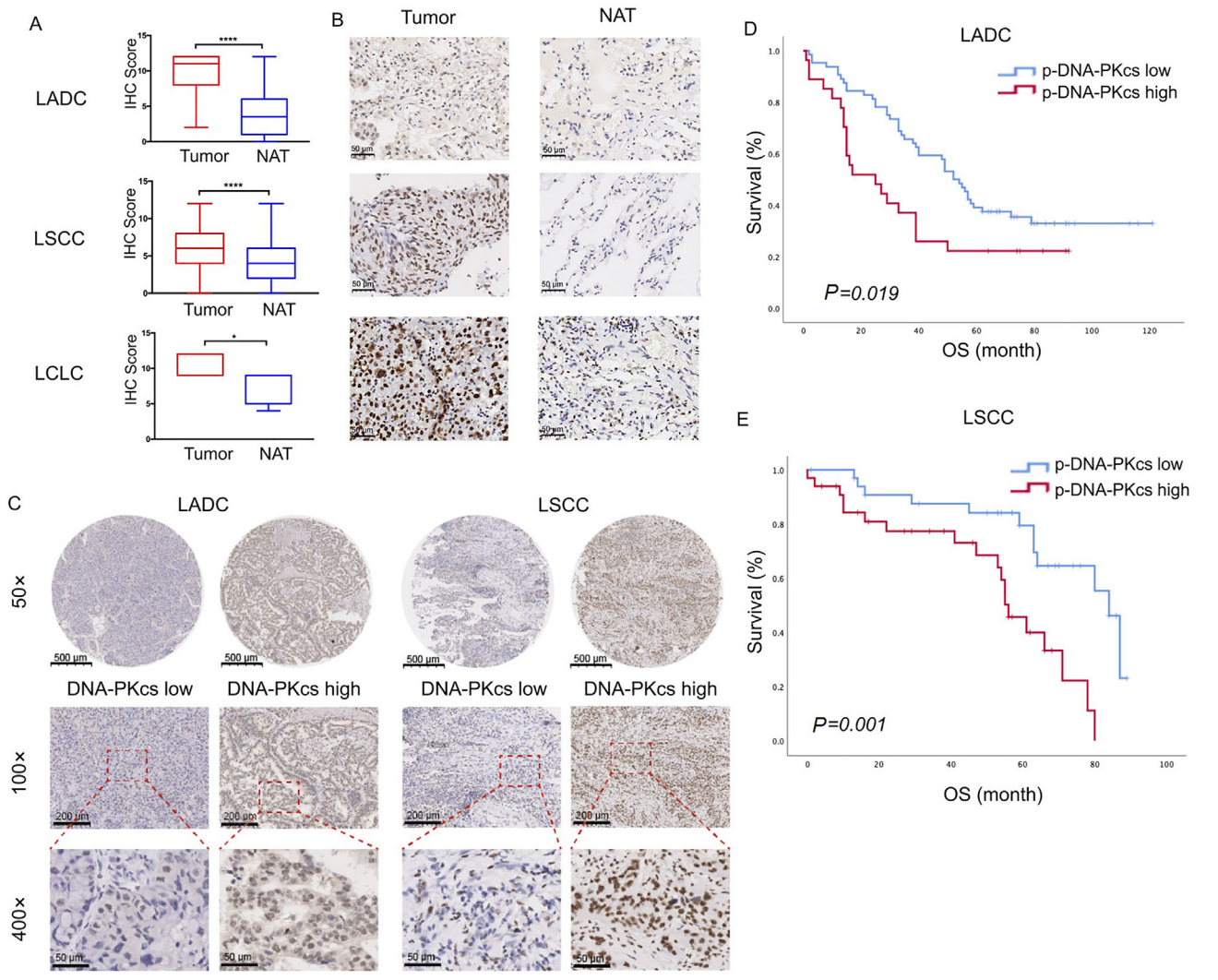

Figure 1 The expression of the catalytic kinase subunit of DNA-dependent protein kinase (DNA-PKcs) in human non-small cell lung cancer (NSCLC) tumor specimens and its correlation with prognosis. (A) and (B) Expression levels of DNA-PKcs in 164 paired NSCLC tumor specimens and their normal tissue adjacent to the tumor (NAT), independently interpreted by two researchers. Data presented as means ± SD [$n = 81$ for lung adenocarcinoma (LADC), $n = 78$ for lung squamous cell carcinoma (LSCC), $n = 5$ for large-cell carcinoma (LCLC), $^{****}P < 0.0001$, $^{*}P < 0.05$], scale bar = 50 μm. (C) Representative immunohistochemical staining for DNA-PKcs in human NSCLC tissues, scale bar = 500 μm (magnification, 50 ×), 100 μm (magnification, 100 ×) and 20 μm (magnification, 400 ×); High/low indicates the expression level of DNA-PKcs in NSCLC tumor microarray. (D) and (E) Kaplan−Meier survival curves of 169 NSCLC (91 LADC and 78 LSCC) patients grouped by nuclear DNA-PKcs expression.

20.05 ± 0.10% in H1703). To provide additional evaluation of cell apoptosis, we conducted TUNEL assay on these three NSCLC cell lines. Results confirm the enhanced apoptosis by M3814 on chemotherapy-treated cells, with higher TUNEL-positive fractions in combination treatment groups (Fig. 3C).

In response to DNA-damaging chemotherapies, sustained G2/M phase growth arrest is often stimulated as a classic cellular response, which allows for cells to repair DNA damage[35]. To provide a potential mechanism for cell growth inhibition induced by the short-term treatments, H460 and A549 cells with indicated treatments were stained with propidium iodide (PI) and analyzed by flow cytometry. Noteworthy, co-therapy with M3814 significantly enhanced the G2/M phase accumulation induced by etoposide in H460 (24.80 ± 3.76% to 64.13 ± 5.64%, $P < 0.001$), A549 cells (20.03 ± 2.16% to 55.5 ± 5.41%, $P < 0.001$), and H1703 cells (25.39 ± 4.84% to 46.40 ± 5.44%, $P < 0.01$) (Fig. 3D and E). Similar trends were observed in paclitaxel treatment, with G2/M fraction rising from 39.13 ± 7.34% to 69.43 ± 13.05% ($P < 0.01$) in A549 cells, 41.10 ± 1.51% to 61.20 ± 2.56% ($P < 0.001$) in H460 cells, and 33.88 ± 2.33% to 45.69 ± 3.15% ($P < 0.01$) in H1703 cells (Fig. 3D and E). Given that persistent G2/M cell cycle arrest was related to a mode of cell death, this finding accorded with our earlier results that short-term combination treatment could induce a prolonged decrease in colony formation. Taken together, these results suggest an irreversible growth arrest in NSCLC cells by M3814−paclitaxel or M3814−etoposide combination by promoting apoptosis and G2/M cell cycle arrest.

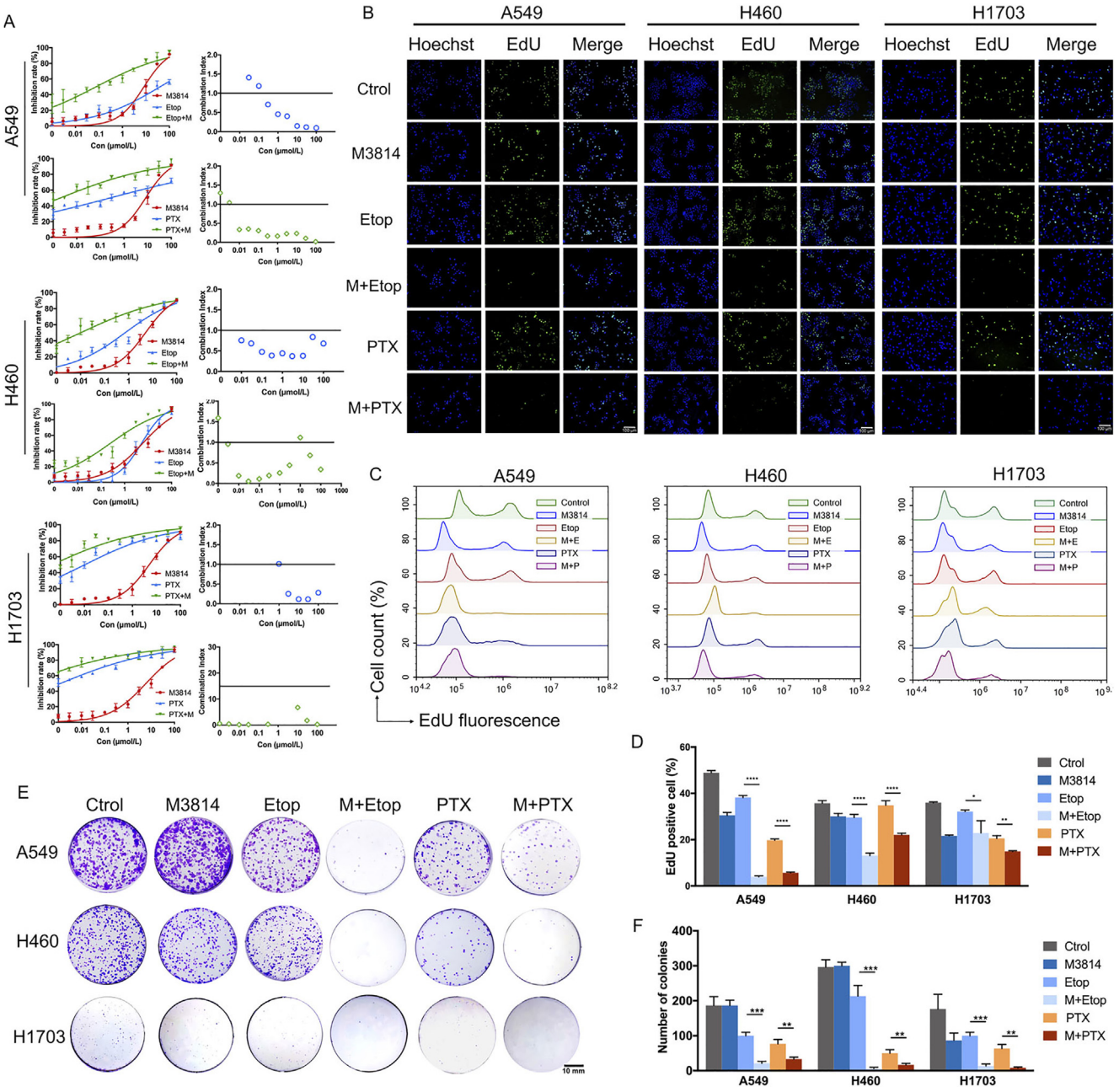

Figure 2 M3814 potentiates the inhibitory effect of chemotherapy on NSCLC cell proliferation *in vitro*. (A) Cell viability curves of NSCLC cell lines A549, H460 and H1703 treated with paclitaxel (PTX) and etoposide (Etop) (concentration gradient from 1 nmol/L to 100 μmol/L), in the absence or presence of M3814 (5 μmol/L) for 48 h. Data are presented as mean ± SD ($n = 3$). The combination index (CI) of the drug combination determined with Chou-Talalay Method. CI < 1 indicates the synergistic effect between M3814 and chemotherapy. (B) Representative images of EdU-DNA incorporation assay in NSCLC cells treated with 5 μmol/L M3814 and 100 nmol/L etoposide for 18 h. EdU staining (green fluorescence), Hoechst staining (blue fluorescence), scale bar = 100 μm (magnification, 100 ×). (C) Flow cytometric analysis of EdU fluorescence. (D) Quantitative data of the EdU-positive fraction. Data presented as mean ± SD ($n = 3$, $^{****}P < 0.0001$, $^{**}P < 0.01$, $^{*}P < 0.05$). (E) and (F) Representative images of colonies (E) and quantitative analyses (F) formation tests in A549, H460 and H1703 cells were treated with paclitaxel (5 nmol/L) and etoposide (100 nmol/L) in the absence or in the presence of M3814 (5 μmol/L) for 18 h, and incubated in 6-well plates for another 14 days. Colonies observed by inverted microscope. Data presented as mean ± SD ($n = 3$, $^{***}P < 0.001$, $^{**}P < 0.01$, $^{*}P < 0.05$).

3.4. M3814 impairs chemotherapy-induced DSB repair by inhibiting DNA-PKcs activation in vitro

γ-H2AX (Ser139) is formed by the phosphorylation of the Ser139 residue of the histone variant H2AX, and is a reliable DSB marker[36]. Given that nearly 20 DSBs are required to achieve the activating threshold of G2/M checkpoint[37], we conducted γ-H2AX (Ser139) immunofluorescence staining to quantify γ-H2AX foci in NSCLC cells. Cells were treated with 100 nmol/L paclitaxel or 1 μmol/L etoposide for 1 h, followed by extensive

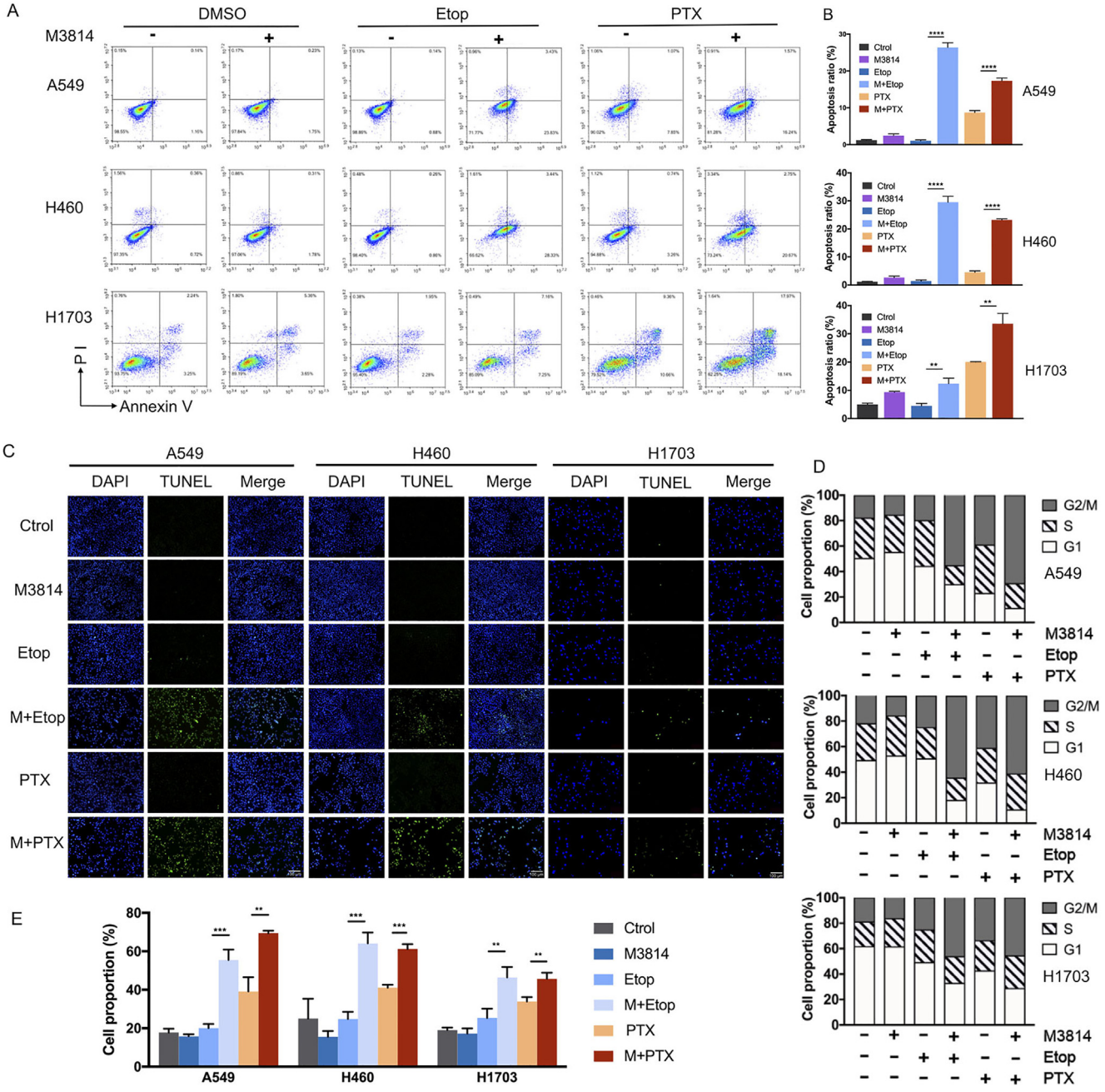

Figure 3 M3814 promotes cell apoptosis and G2/M cell cycle arrest induced by chemotherapy *in vitro*. (A) NSCLC cell lines A549, H460 and H1703 were treated with paclitaxel (5 nmol/L) and etoposide (100 nmol/L) with or without M3814 (5 μmol/L) for 48 h, stained with Annexin V/PI and evaluated through flow cytometry. (B) Quantitative analysis of apoptotic cell proportion. Apoptotic cells included those with Annexin V^+/PI^- and Annexin V^+/PI^+ labelling. Data presented as means ± SD ($n = 3$, $^{****}P < 0.0001$, $^{**}P < 0.01$). (C) Representative immunofluorescent images of TUNEL staining at 48 h following indicated treatment. TUNEL staining (green), DAPI staining (blue), scale bar = 100 μm (magnification, 100 ×). (D) Cell cycle distribution detected by flow cytometry analyses on A549 and H460 cells. Cells were treated with paclitaxel (5 nmol/L) and etoposide (100 nmol/L) with or without M3814 (5 μmol/L), and stained with propidium iodide (PI) at 12 h post-treatment. (E) Quantitative analysis of G2/M fraction of NSCLC cells with indicated treatments. Data are presented as mean ± SD ($n = 3$, $^{***}P < 0.001$, $^{**}P < 0.01$).

washing in drug-free medium, and incubation with or without 5 μmol/L M3814 for another 4 h. We noticed a rapid induction of DNA damage by either 100 nmol/L paclitaxel or 1 μmol/L etoposide, with a more striking increase in the number of γ-H2AX foci observed in the combination group (Fig. 4A). Compared with etoposide or paclitaxel monotherapy, the addition of M3814 significantly increased the number of γ-H2AX foci per cell following paclitaxel ($P = 0.007$ in A549 cells and $P = 0.016$ in H460 cells) and etoposide treatment ($P = 0.011$ in A549 cells and $P = 0.044$ in H460 cells) (Fig. 4B).

The efficiency of DSB induction and its subsequent repair substantially determines the efficacy of chemotherapy in tumor

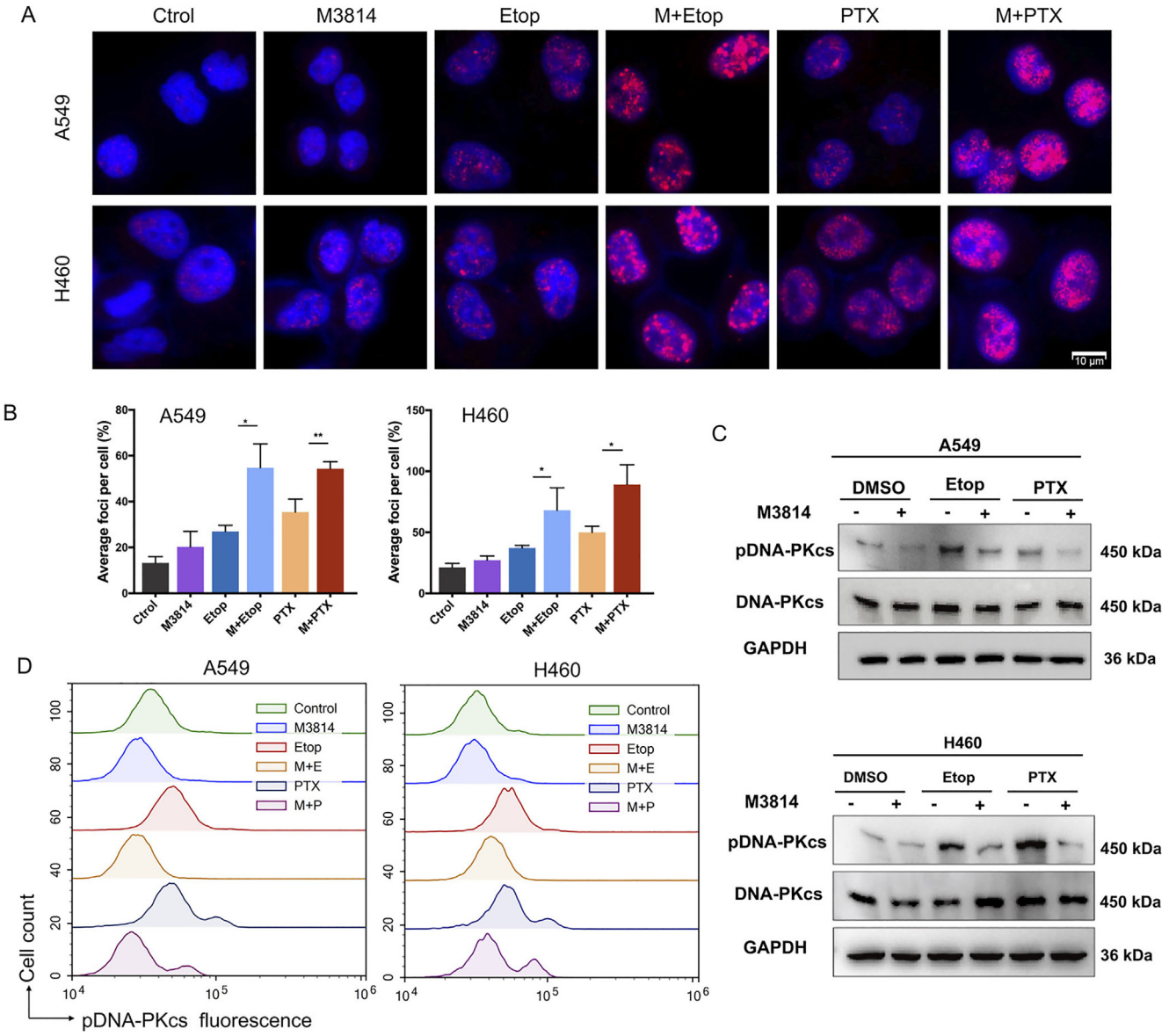

Figure 4 M3814 impairs chemotherapy-induced double-strand breaks (DSBs) repair by inhibiting DNA-PKcs activation *in vitro*. (A) Representative images of NSCLC cells incubated in the presence or absence of 5 μmol/L M3814 for 1 h before adding 100 nmol/L paclitaxel or 1 μmol/L etoposide. Following extensive washing in drug-free medium, cells were incubated with or without 5 μmol/L M3814 for another 4 h, and immunostained for γ-H2AX (red) foci. DAPI staining (blue fluorescence), scale bar = 10 μm (magnification, 1000 ×). (B) Quantitative analysis of γ-H2AX foci per cells. Data are presented as mean ± SD ($n = 3$, $^{**}P < 0.01$, $^{*}P < 0.05$). (C) The phosphorylation of DNA-PKcs and the expression of total-DNA-PKcs were determined by Western blot analysis on NSCLC cells with indicated treatment. (D) Flow cytometric analysis of phospho-DNA-PKcs fluorescence.

cells. DNA-PKcs activation can be evaluated by the phosphorylation of catalytic subunit DNA-PKcs at Ser2056 site. Notably, Western blot results reveal no significant change in protein expression of total-DNA-PKcs, but suggest a rapid up-regulation of p-DNA-PK (Ser2056) expression in cells treated with chemotherapy (Fig. 4C). However, compared with paclitaxel or etoposide monotherapy, the addition of M3814 significantly inhibited the autophosphorylation of DNA-PKcs induced by chemotherapy, as evidenced by the relatively lower protein expression of p-DNA-PKcs in cells with concomitant treatment, which was further solidified by p-DNA-PKcs flow cytometry assay where M3814 prevented the increase of p-DNA-PKcs (Ser2056) fluorescence in chemotherapy-treated cells (Fig. 4D). These results collectively suggest that chemotherapy-induced DNA damage led to DNA-PKcs autophosphorylation so as to initiate DSBs repair in tumor cells, which was nevertheless suppressed by M3814. Thus, DNA-PK inhibitor M3814 impaired the DSB-repair machinery in NSCLC cells through the down-regulation of p-DNA-PKcs (Ser2056).

3.5. P53-dependent accelerated senescence response by M3814 following chemotherapy treatment

On the basis of early knowledge that delayed DSB repair contributes to cellular senescence, which has historically been characterized as a predominant change during irreversible cell-cycle

arrest[38], we subjected post-treatment NSCLC cells to senescence-associated β-galactosidase (SA-βGal) staining assays. In both H460 and A549 cell lines, single treatment with M3814 or chemotherapy failed to induce substantial senescence response relative to untreated controls (Fig. 5A). On the other hand, the concomitant treatment with M3814 and chemotherapy significantly increased the SA-βGal-positive fraction ($P < 0.001$ in paclitaxel group, and $P < 0.0001$ in etoposide group), indicating a synergistic promotion of senescence by M3814 and chemotherapy (Fig. 5B). Noteworthy, SA-βGal-positive cells exhibited characteristic morphologic features of senescence, including cell enlargement, elongation, and multinucleation (Fig. 5A). Cellular senescence induced by DNA damage response in human cells is typically characterized by the upregulation of P53[39–42]. We

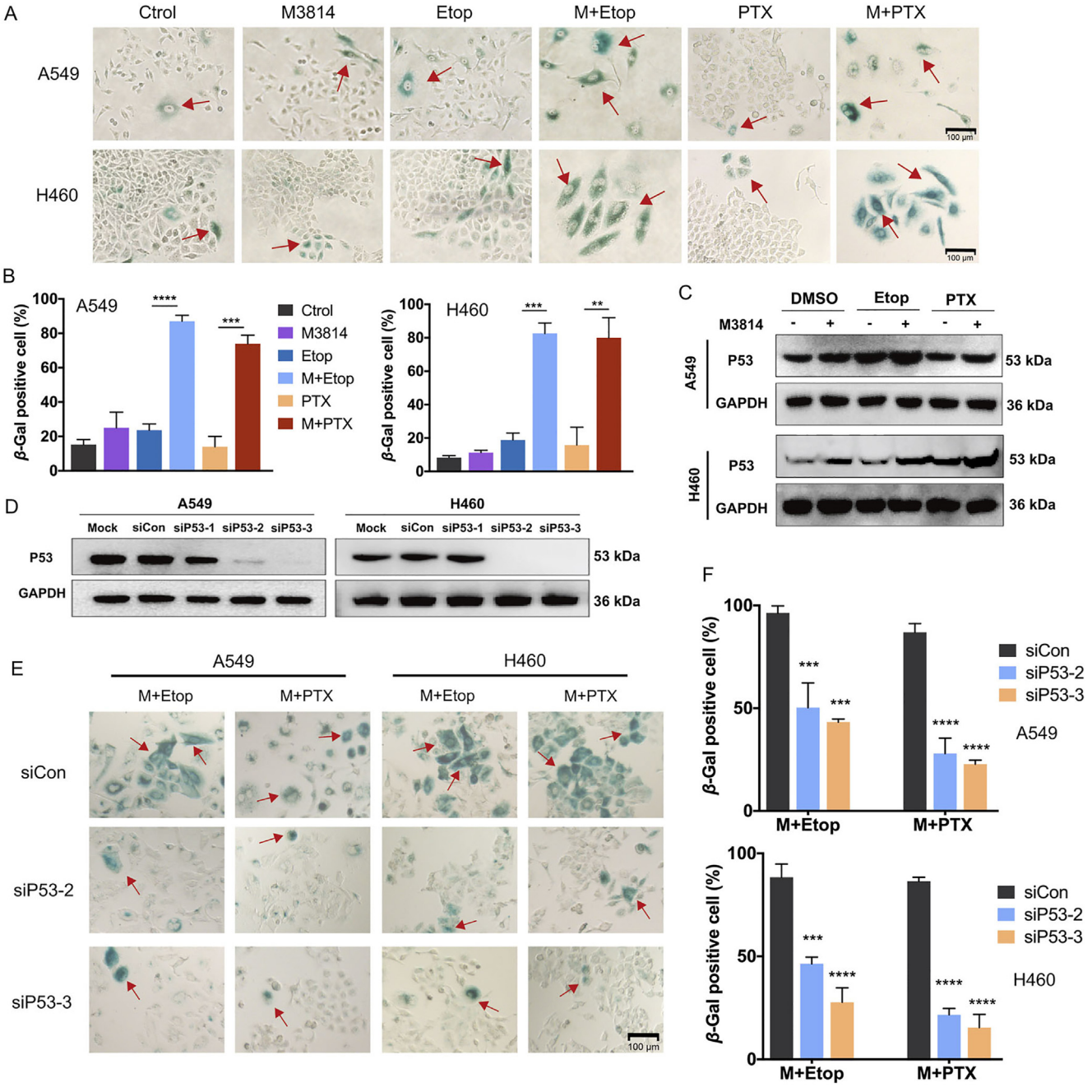

Figure 5 P53-dependent accelerated senescence response by M3814 following chemotherapy treatment. (A) Representative images of senescence-associated beta-galactosidase (SA-βgal) activity in NSCLC cells after 24 h of indicated treatment followed by another 72 h incubation. Scale bar = 100 μm (magnification, 100 ×). (B) Quantitative analysis of SA-βGal positive cells. Data are presented as mean ± SD ($n = 3$, $^{****}P < 0.0001$, $^{***}P < 0.001$, $^{**}P < 0.01$). (C) Western blot assays on P53 expressions in H460 and A549 cells at 12 h post-treatment. (D) Expression levels of P53 determined by Western blot analyses at 72 h post-transfection for the selection of candidate siRNA-*P53*. (E) Representative images of SA-βGal activity in NSCLC cells transfected with siRNA-control and two siRNA-*P53*. Scale bar = 100 μm (magnification, 100 ×). (F) Quantitative analysis of SA-βGal positive cells. Data are presented as mean ± SD ($n = 3$, $^{****}P < 0.0001$, $^{***}P < 0.001$).

identified a significant upregulation of P53 protein expression in combination treatment groups by Western blot analyses (Fig. 5C).

As both A549 and H460 cells are P53-wild-type[43], we investigated whether the accelerated senescence induced by M3814 in chemotherapy-treated cells is P53 dependent. Expression levels of P53 were analyzed 72 h post-transfection by Western blot and two candidate siRNA-P53 were selected (Fig. 5D). Although both M3814−paclitaxel and M3814−etoposide combination led to notable SA-βGal staining in P53 wild-type A549 and H460 cells, the accelerated senescence was significantly weakened by siRNA knock-down of P53 (Fig. 5E and F). Together, these findings collectively suggest that the accelerated senescence response of NSCLC cells following M3814+chemotherapy combination is P53-dependent.

3.6. *M3814 potentiates the antitumor activities of chemotherapy in NSCLC xenograft models*

The preliminary *in vitro* success motivated further research on the chemosensitization effect of M3814 *in vivo*. We evaluated the anti-tumor efficacy of M3814 and chemotherapy in two subcutaneous NSCLC xenograft models (Figs. 6 and 7). To elicit a measurable antitumor activity without inducing significant toxicity, treatment regimens include a suggested dose of etoposide (10 mg/kg i.p.) every three days[44,45] and a tolerated dose of M3814 (40 mg/kg) orally administrated once daily. At the end of experiment, tumors from control groups of A549 and H460 models reached 6.34 ± 1.35 and 15.95 ± 2.95 times their starting volume (RTV6.34 and RTV15.95), respectively (Fig. 6A). As shown in Fig. 6B−E, combinational treatment with M3814 and etoposide substantially delayed tumor growth compared with either treatment alone. As for the anti-tumor effect of M3814+paclitaxel *in vivo*, we found that M3814 administered orally at a tolerated dose of 40 mg/kg once daily further enhanced the treatment response to paclitaxel (10 mg/kg i.p. once every three days) in mice implanted with A549 and H460 xenografts (Fig. 7A). Whereas M3814 monotherapy induced tumor growth inhibition in A549 xenograft model, H460 tumors were insensitive to M3814 single treatment (Fig. 7B−E).

Immunohistochemical analyses were used to evaluate tumor cell proliferation *in vivo*, characterized by Ki67-positive rates in xenografts. As shown in Figs. 6F and 7F, concomitant use of M3814 and chemotherapy decreased Ki67 expression in tumor tissues relative to controls. Tumor tissues were also subjected to TUNEL staining assays for the detection of apoptotic DNA fragmentation. Though chemotherapy treatment alone upregulated TUNEL staining in tumor tissues, the effect was most pronounced in the combination group, which was in accordance with our *in vitro* results that M3814 worked synergistically with chemotherapy to induce apoptosis. Comparable with *in vitro* results, the addition of M3814 elevated γ-H2AX (Ser139) levels relative to chemotherapy treatment alone. Moreover, we observed an increase in p-DNA-PK (Ser2056) in xenografts treated with chemotherapy, which was abolished by the additional treatment with M3814. We then examined SA-βGal activities in A549 xenografts to validate the senescence-inducing effect of the drug combination *in vitro*. Tumors treated with M3814 monotherapy displayed minimal SA-βGal staining whereas tumors from

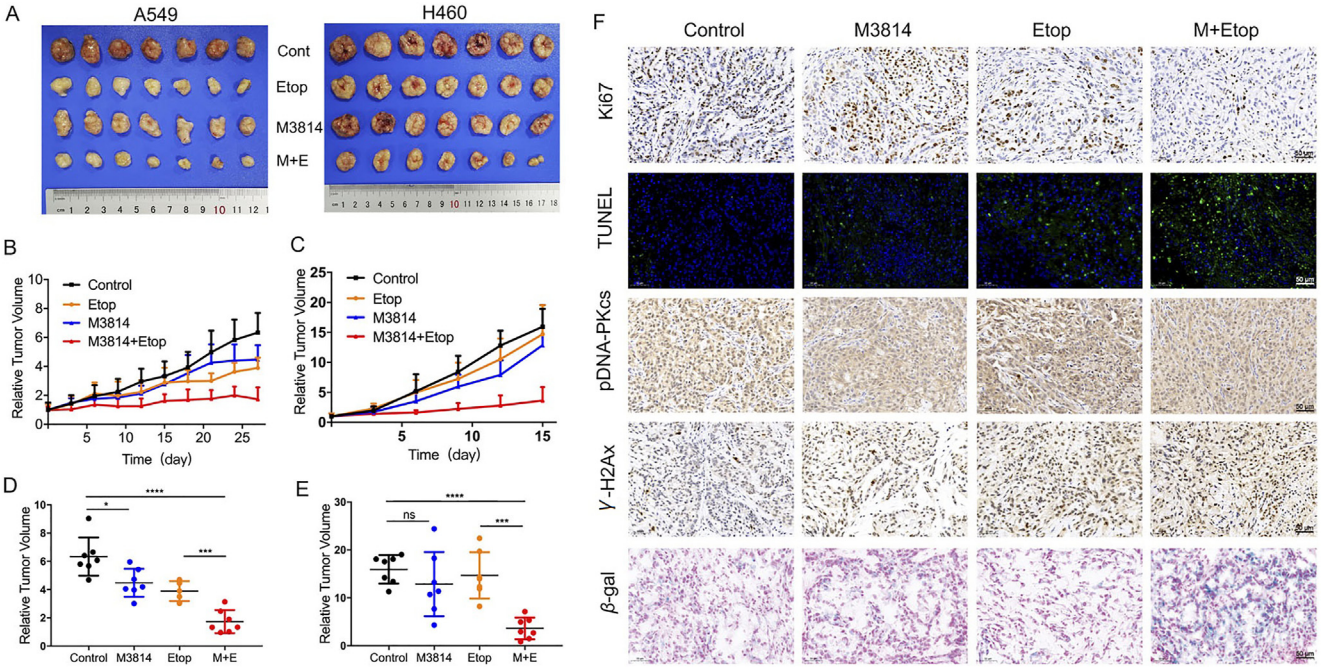

Figure 6 The synergistic anti-tumor effect of M3814 and etoposide in NSCLC xenografts. NOD-SCID mice implanted with A549 and H460 tumor xenografts were treated with M3814 (50 mg/kg, i.g. daily) and etoposide (10 mg/kg, i.p. once 3 days). (A) Subcutaneous A549 and H460 tumors at the end of this experiment. (B) and (C) Growth of A549 and H460 xenografts presented as mean RTV (relative tumor volume). Error bars denote SD. (D) and (E) The final RTV of xenograft tumors measured in each group. Data are presented as mean ± SD ($n = 7$, $^{****}P < 0.0001$, $^{***}P < 0.001$, $^{*}P < 0.05$; ns, $P > 0.05$). (F) Representative images of immunohistochemistry staining of Ki67, γ-H2AX, pDNA-PKcs and immunofluorescence staining of TUNEL evaluated on paraffin-embedded A549 tumor sections, scale bar = 50 μm (magnification, 200 ×). Representative images of SA-βGal staining of frozen sections of A549 tumors, scale bar = 50 μm (magnification, 200 ×).

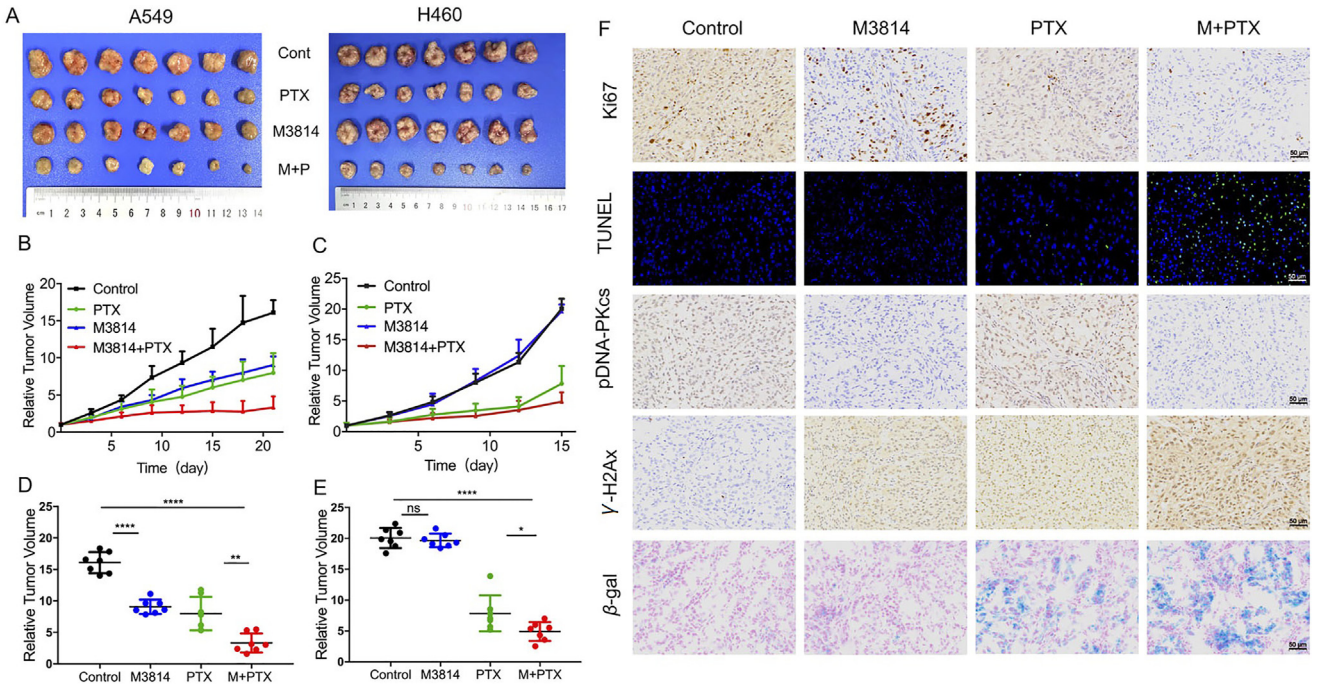

Figure 7 The synergistic anti-tumor effect of M3814 and paclitaxel in NSCLC xenografts. NOD-SCID mice implanted with A549 and H460 tumor xenografts were treated with M3814 (50 mg/kg, i.g. daily) and paclitaxel (10 mg/kg, i.v. once 3 days). (A) Subcutaneous A549 and H460 tumors at the end of this experiment. (B) and (C) Growth of A549 and H460 xenografts presented as mean RTV (relative tumor volume). Error bars denote SD. (D) and (E) The final RTV of xenograft tumors measured in each group. Data are presented as mean ± SD ($n = 7$, $^{****}P < 0.0001$, $^{***}P < 0.001$, $^{**}P < 0.01$, $^{*}P < 0.05$; ns, $P > 0.05$). (F) Representative images of immunohistochemistry staining of Ki67, γ-H2AX, pDNA-PKcs and immunofluorescence staining of TUNEL evaluated on paraffin-embedded A549 tumor sections, scale bar = 50 μm (magnification, 200 ×). Representative images of SA-βGal staining of frozen sections of A549 tumors, scale bar = 50 μm (magnification, 200 ×).

combination treatment groups demonstrated significantly higher SA-βGal positivity (Figs. 6F and 7F). This evidence collectively reveals the chemosensitization efficacy of M3814 in NSCLC xenograft models, through the suppression of tumor cell proliferation, and the induction of apoptosis, DNA damage and cell senescence.

3.7. *Toxicity evaluation*

In the four combinations based on two NSCLC xenograft models and two chemotherapy, single use of M3814 did not induce unacceptable toxicity. Though A549 xenograft mice treated with etoposide monotherapy experienced body weight loss compared with control group mice (maximum body weight loss <20%, final body weight >18 g; Supporting Information Fig. S2), co-therapy with M3814 did not induce further weight loss. It is thus interesting to speculate whether the body weight loss caused by combinational treatment was attributed to the potential toxicity of etoposide. To further assess the *in vivo* safety of the treatment, we performed blood biochemical analyses, which revealed no significant differences in biochemical indexes between groups (Fig. S2).

4. Discussion

A large proportion of NSCLC patients are ineligible for operations due to late diagnosis. Recent attempts have thus converged on systemic treatments based on chemotherapies and target therapies[46]. Currently etoposide-cisplatin (EP) and carboplatin-paclitaxel (PC) regimens remain the two most commonly-used concurrent regimens for advanced NSCLC patients[47,48]. Although these two regimes have been extensively applied in clinical practice, accumulating side effects due to large doses and frequently-developed chemoresistance have made the treatment results suboptimal. Old-generation DNA-PK inhibitors have been proved effective but are limited in terms of selectivity due to structural similarities with PI3Ks. M3814 represents the new-generation of selective DNA-PK protein kinase inhibitors. To the best of our knowledge, this is the first study to systematically evaluate the chemosensitization effect of M3814 on paclitaxel and etoposide in NSCLC models, both *in vitro* and *in vivo*. The present study provides a theoretical basis for the use of M3814 in combination with chemotherapy in clinical practice, with which we hope to aid the optimization of NSCLC treatment.

We identified enhanced cytotoxic effect by M3814 in NSCLC cell lines treated with paclitaxel and etoposide, both *in vitro* and *in vivo*. CCK8 assay results reveal a synergistic inhibition (CI < 1) of M3814 combined with low, noncytotoxic concentrations of etoposide and paclitaxel. The direct detection of tumor cell DNA synthesis is the most accurate way to evaluate cell proliferation[49]. In recent years, the EdU assay is more often used than the BrdU (bromo deoxyuridine) method for the detection of DNA synthesis, due to the fact that EdU method does not require antibody reaction

and demonstrates higher detection sensitivity. EdU is a thymine nucleoside analogue and can be inserted into the replicating DNA when tumor cells proliferate, thus directly reflecting DNA replication activity. Compared with monotherapy, we observed a significantly smaller number of EdU positive cells in the combination treatment group, suggesting that concomitant treatments with chemotherapies and M3814 could inhibit NSCLC cell proliferation by disrupting the DNA synthesis. Based on the promising inhibition synergy between M3814 and chemotherapeutic agents *in vitro*, animal studies using A549 and H460 human NSCLC xenograft systems were conducted. In the four combinations based on two NSCLC xenograft models and two chemotherapies, we also observed tumor regression at tolerated doses *in vivo*.

DNA double-strand breaks (DSBs) are considered the most lethal form of DNA lesions, and can be induced by genotoxic agents such as chemotherapeutic agents used in cancer treatments[50]. γ-H2AX (Ser139) is formed by the phosphorylation of the Ser139 residue of the histone variant H2AX, and is commonly used to measure early cellular response to DSB stimulants[51]. Recently, growing evidence suggests that paclitaxel could induce cellular DNA damage[52−55]. In line with these results, we noticed a rapid induction of DNA damage by short-term treatment (1 h) of high concentration of paclitaxel (100 nmol/L), with more striking DNA-damage induction observed in the combination group. Moreover, the induction of DNA damage by paclitaxel was further proved by the phosphorylation of DNA-PKcs, suggesting that DNA damage caused by paclitaxel initiated the DNA repair process in tumor cells. The efficiency of DSB induction and its subsequent repair substantially determines the efficacy of chemotherapy in tumor cells. A pivotal mechanism for DNA repair in mammals is the activation of DNA-PKcs at DSB sites[56]. Multiple phosphorylation sites of DNA-PKcs have continuously been identified including serine 2056 (Ser2056), the phosphorylation of which is essential to NHEJ pathway by preventing DNA end processing[57,58]. Our results reveal no significant change in protein expression of total-DNA-PKcs after treatment with M3814+etoposide for 4 h. On the other hand, the expression of p-DNA-PK (Ser2056) was down-regulated by combined treatment relative to chemotherapy alone, suggesting a potential mechanism for this drug synergy that M3814 impaired the DSB-repair machinery of NSCLC cells by suppressing the phosphorylation of DNA-PKcs.

Conventional anti-cancer treatments such as certain types of chemotherapy are built on the premise of enhanced DNA damage-related cell death, which may lead to serious side effects or commonly-developed chemoresistance[59]. Instead of directly causing cytotoxic cell death, some treatment modalities aim to permanently inhibit cancer cell proliferation by stimulating growth arrest. In this study, we found that both paclitaxel and etoposide work synergistically with M3814 to induce cellular senescence so as to inhibit tumor growth. Persistent G2/M cell cycle arrest is a classic cellular response to DNA damage[35], allowing the repair of DSBs before cell enter mitosis and thus maintaining genomic stability of cells[60−63]. In the present study, we found that the chemosensitization effect of M3814 was accompanied by an increased level of G2−M cell cycle arrest. Accumulating evidence suggests that cell cycle arrest contributes to tumor cell senescence[64], which can be triggered by the delayed repair of DSBs[65,66] and is thus considered as a potential mechanism for tumor inhibition. The senescent cells were large in size and expressed high activity β-galactosidase at pH 6.0. We observed higher levels of β-galactosidase staining in cells treated with chemotherapy−M3814 combination than with either monotherapy. Similar findings have previously been addressed that the selective knockout of DNA-PK could induce accelerated senescence of cancer cells after radiotherapy[39]. Cell senescence induced by DNA damage response in human cells is typically characterized by the upregulation of P53[39−42]. We found that the accelerated cell senescence induced by combination treatments was significantly weakened by siRNA knock-down of P53. These findings collectively reveal a P53-dependent accelerated senescence response by M3814 following treatment with paclitaxel/etoposide.

The results of this study highlight the therapeutic potential of combining DNA-PK blockade with chemotherapy in human NSCLC. To the best of our knowledge, this is the first study to systematically evaluate the chemosensitization effect of M3814, a new-generation selective DNA-PK inhibitors in NSCLC models, both *in vitro* and *in vivo*. Importantly, multiple anti-tumor modalities of M3814−chemotherapy combination were identified including direct cytotoxic cell death, and permanent growth arrest.

5. Conclusions

The new-generation DNA-PK selective inhibitor M3814 potentiates the anti-tumor effect of paclitaxel and etoposide in A549 and H460 human NSCLC cell lines. Tumor regression was also observed at tolerated doses *in vivo*. The accelerated senescence of NSCLC cells induced by M3814−chemotherapy combination was P53-dependent, indicating a potential explanation for the anti-tumor effect of this drug synergy. The present study provides a theoretical basis for the use of M3814 in combination with paclitaxel and etoposide in clinical practice, which warrants further evaluation and would hopefully aid the optimization of NSCLC treatment.

Acknowledgments

This work is supported by the National Natural Science Foundation Regional Innovation and Development (U19A2003, China) and by the Excellent Youth Foundation of Sichuan Scientific Committee Grant in China (No. 2019JDJQ008).

Author contributions

Manni Wang and Siyuan Chen conducted experiments, analyzed data, and wrote the manuscript. Yuquan Wei and Xiawei Wei provided conceptual idea and cost, guided the project and revised the manuscript. The authors read and approved the final manuscript.

Conflicts of interest

The authors declare no competing interests.

Appendix A. Supporting information

Supporting data to this article can be found online at https://doi.org/10.1016/j.apsb.2021.07.029.

References

1. Gerard C, Debruyne C. Immunotherapy in the landscape of new targeted treatments for non-small cell lung cancer. *Mol Oncol* 2009;**3**:409−24.
2. Sandler AB. Chemotherapy for small cell lung cancer. *Semin Oncol* 2003;**30**:9−25.
3. Lackey A, Donington JS. Surgical management of lung cancer. *Semin Intervent Radiol* 2013;**30**:133−40.
4. Mountain CF, Dresler CM. Regional lymph node classification for lung cancer staging. *Chest* 1997;**111**:1718−23.
5. Johnston SR. Ovarian cancer: review of the national institute for clinical excellence (NICE) guidance recommendations. *Cancer Invest* 2004;**22**:730−42.
6. Ward JF. The yield of DNA double-strand breaks produced intracellularly by ionizing radiation: a review. *Int J Radiat Biol* 1990;**57**:1141−50.
7. Iliakis G. The role of DNA double strand breaks in ionizing radiation-induced killing of eukaryotic cells. *Bioessays* 1991;**13**:641−8.
8. Zhuang W, Li B, Long L, Chen L, Huang Q, Liang Z. Induction of autophagy promotes differentiation of glioma-initiating cells and their radiosensitivity. *Int J Cancer* 2011;**129**:2720−31.
9. Mao Z, Bozzella M, Seluanov A, Gorbunova V. DNA repair by nonhomologous end joining and homologous recombination during cell cycle in human cells. *Cell Cycle* 2008;**7**:2902−6.
10. Mahaney BL, Meek K, Lees-Miller SP. Repair of ionizing radiation-induced DNA double-strand breaks by non-homologous end-joining. *Biochem J* 2009;**417**:639−50.
11. Lieber MR. The mechanism of human nonhomologous DNA end joining. *J Biol Chem* 2008;**283**:1−5.
12. Chan DW, Chen BP, Prithivirajsingh S, Kurimasa A, Story MD, Qin J, et al. Autophosphorylation of the DNA-dependent protein kinase catalytic subunit is required for rejoining of DNA double-strand breaks. *Genes Dev* 2002;**16**:2333−8.
13. Gottlieb TM, Jackson SP. The DNA-dependent protein kinase: requirement for DNA ends and association with Ku antigen. *Cell* 1993;**72**:131−42.
14. Davidson D, Amrein L, Panasci L, Aloyz R. Small molecules, inhibitors of DNA-PK, targeting DNA repair, and beyond. *Front Pharmacol* 2013;**4**:5.
15. Mari PO, Florea BI, Persengiev SP, Verkaik NS, Bruggenwirth HT, Modesti M, et al. Dynamic assembly of end-joining complexes requires interaction between Ku70/80 and XRCC4. *Proc Natl Acad Sci U S A* 2006;**103**:18597−602.
16. Britton S, Coates J, Jackson SP. A new method for high-resolution imaging of Ku foci to decipher mechanisms of DNA double-strand break repair. *J Cell Biol* 2013;**202**:579−95.
17. Shao Z, Davis AJ, Fattah KR, So S, Sun J, Lee KJ, et al. Persistently bound Ku at DNA ends attenuates DNA end resection and homologous recombination. *DNA Repair* 2012;**11**:310−6.
18. Uematsu N, Weterings E, Yano K, Morotomi-Yano K, Jakob B, Taucher-Scholz G, et al. Autophosphorylation of DNA-PKCS regulates its dynamics at DNA double-strand breaks. *J Cell Biol* 2007;**177**:219−29.
19. Cary RB, Peterson SR, Wang J, Bear DG, Bradbury EM, Chen DJ. DNA looping by Ku and the DNA-dependent protein kinase. *Proc Natl Acad Sci U S A* 1997;**94**:4267−72.
20. DeFazio LG, Stansel RM, Griffith JD, Chu G. Synapsis of DNA ends by DNA-dependent protein kinase. *EMBO J* 2002;**21**:3192−200.
21. Weterings E, van Gent DC. The mechanism of non-homologous end-joining: a synopsis of synapsis. *DNA Repair* 2004;**3**:1425−35.
22. Yoo S, Dynan WS. Geometry of a complex formed by double strand break repair proteins at a single DNA end: recruitment of DNA-PKcs induces inward translocation of Ku protein. *Nucleic Acids Res* 1999;**27**:4679−86.
23. Calsou P, Frit P, Humbert O, Muller C, Chen DJ, Salles B. The DNA-dependent protein kinase catalytic activity regulates DNA end processing by means of Ku entry into DNA. *J Biol Chem* 1999;**274**:7848−56.
24. Xing J, Wu X, Vaporciyan AA, Spitz MR, Gu J. Prognostic significance of ataxia-telangiectasia mutated, DNA-dependent protein kinase catalytic subunit, and Ku heterodimeric regulatory complex 86-kD subunit expression in patients with nonsmall cell lung cancer. *Cancer* 2008;**112**:2756−64.
25. Shintani S, Mihara M, Li C, Nakahara Y, Hino S, Nakashiro K, et al. Up-regulation of DNA-dependent protein kinase correlates with radiation resistance in oral squamous cell carcinoma. *Cancer Sci* 2003;**94**:894−900.
26. Tian X, Chen G, Xing H, Weng D, Guo Y, Ma D. The relationship between the down-regulation of DNA-PKcs or Ku70 and the chemosensitization in human cervical carcinoma cell line HeLa. *Oncol Rep* 2007;**18**:927−32.
27. Beskow C, Skikuniene J, Holgersson A, Nilsson B, Lewensohn R, Kanter L, et al. Radioresistant cervical cancer shows upregulation of the NHEJ proteins DNA-PKcs, Ku70 and Ku86. *Br J Cancer* 2009;**101**:816−21.
28. Bouchaert P, Guerif S, Debiais C, Irani J, Fromont G. DNA-PKcs expression predicts response to radiotherapy in prostate cancer. *Int J Radiat Oncol Biol Phys* 2012;**84**:1179−85.
29. Fok JHL, Ramos-Montoya A, Vazquez-Chantada M, Wijnhoven PWG, Follia V, James N, et al. AZD7648 is a potent and selective DNA-PK inhibitor that enhances radiation, chemotherapy and olaparib activity. *Nat Commun* 2019;**10**:5065.
30. Fuchss T, Mederski WW, Emde U, Buchstallter H-P, Zenke F, Zimmermann A, et al. Abstract 4198: highly potent and selective DNA-PK inhibitor M3814 with sustainable anti-tumor activity in combination with radiotherapy. *Cancer Res* 2017;**77**:4198.
31. Wise HC, Iyer GV, Moore K, Temkin SM, Gordon S, Aghajanian C, et al. Activity of M3814, an oral DNA-PK inhibitor, in combination with topoisomerase II inhibitors in ovarian cancer models. *Sci Rep* 2019;**9**:18882.
32. Zimmermann A, Carr M, Zenke FT, Blaukat A, Vassilev LT. Abstract 269: DNA-PK inhibitor, M3814, as a new combination partner of mylotarg in the treatment of acute myeloid leukemia. *Cancer Res* 2019;**79**:269.
33. Klein C, Dokic I, Mairani A, Mein S, Brons S, Häring P, et al. Overcoming hypoxia-induced tumor radioresistance in non-small cell lung cancer by targeting DNA-dependent protein kinase in combination with carbon ion irradiation. *Radiat Oncol* 2017;**12**:208.
34. Chou TC, Talalay P. Quantitative analysis of dose-effect relationships: the combined effects of multiple drugs or enzyme inhibitors. *Adv Enzym Regul* 1984;**22**:27−55.
35. Bunz F, Dutriaux A, Lengauer C, Waldman T, Zhou S, Brown JP, et al. Requirement for p53 and p21 to sustain G2 arrest after DNA damage. *Science* 1998;**282**:1497−501.
36. Mah LJ, El-Osta A, Karagiannis TC. gammaH2AX: a sensitive molecular marker of DNA damage and repair. *Leukemia* 2010;**24**:679−86.
37. Deckbar D, Birraux J, Krempler A, Tchouandong L, Beucher A, Walker S, et al. Chromosome breakage after G2 checkpoint release. *J Cell Biol* 2007;**176**:749−55.
38. Lopez-Otin C, Blasco MA, Partridge L, Serrano M, Kroemer G. The hallmarks of aging. *Cell* 2013;**153**:1194−217.
39. Azad A, Jackson S, Cullinane C, Natoli A, Neilsen PM, Callen DF, et al. Inhibition of DNA-dependent protein kinase induces accelerated senescence in irradiated human cancer cells. *Mol Cancer Res* 2011;**9**:1696−707.
40. Campisi J, d'Adda di Fagagna F. Cellular senescence: when bad things happen to good cells. *Nat Rev Mol Cell Biol* 2007;**8**:729−40.
41. Shay JW, Roninson IB. Hallmarks of senescence in carcinogenesis and cancer therapy. *Oncogene* 2004;**23**:2919−33.
42. Aliouat-Denis CM, Dendouga N, Van den Wyngaert I, Goehlmann H, Steller U, van de Weyer I, et al. p53-independent regulation of p21Waf1/Cip 1 expression and senescence by Chk2. *Mol Cancer Res* 2005;**3**:627−34.

43. Senoo M, Tsuchiya I, Matsumura Y, Mori T, Saito Y, Kato H, et al. Transcriptional dysregulation of the p73L/p63/p51/p40/KET gene in human squamous cell carcinomas: expression of Delta Np73L, a novel dominant-negative isoform, and loss of expression of the potential tumour suppressor p51. *Br J Cancer* 2001;**84**:1235−41.
44. Drapkin BJ, George J, Christensen CL, Mino-Kenudson M, Dries R, Sundaresan T, et al. Genomic and functional fidelity of small cell lung cancer patient-derived xenografts. *Cancer Discov* 2018;**8**:600−15.
45. Zhao Y, Thomas HD, Batey MA, Cowell IG, Richardson CJ, Griffin RJ, et al. Preclinical evaluation of a potent novel DNA-dependent protein kinase inhibitor NU7441. *Cancer Res* 2006;**66**:5354−62.
46. Qin S, Yu H, Wu X, Luo Z, Wang H, Sun S, et al. Weekly albumin-bound paclitaxel/cisplatin versus gemcitabine/cisplatin as first-line therapy for patients with advanced non-small-cell lung cancer: a phase II open-label clinical study. *Chin J Cancer Res* 2019;**31**:339−48.
47. Liang J, Bi N, Wu S, Chen M, Lv C, Zhao L, et al. Etoposide and cisplatin *versus* paclitaxel and carboplatin with concurrent thoracic radiotherapy in unresectable stage III non-small cell lung cancer: a multicenter randomized phase III trial. *Ann Oncol* 2017;**28**:777−83.
48. Eberhardt WE. Concurrent chemoradiotherapy in stage III non-small-cell lung cancer: what is the best regimen?. *J Clin Oncol* 2015;**33**:532−3.
49. Madhavan H. Simple laboratory methods to measure cell proliferation using DNA synthesis property. *J Stem Cells Regen Med* 2007;**3**:12−4.
50. Lama-Sherpa TD, Shevde LA. An Emerging regulatory role for the tumor microenvironment in the DNA damage response to double-strand breaks. *Mol Cancer Res* 2020;**18**:185−93.
51. Redon C, Pilch D, Rogakou E, Sedelnikova O, Newrock K, Bonner W. Histone H2A variants H2AX and H2AZ. *Curr Opin Genet Dev* 2002;**12**:162−9.
52. Branham MT, Nadin SB, Vargas-Roig LM, Ciocca DR. DNA damage induced by paclitaxel and DNA repair capability of peripheral blood lymphocytes as evaluated by the alkaline comet assay. *Mutat Res* 2004;**560**:11−7.
53. Mikula-Pietrasik J, Witucka A, Pakula M, Uruski P, Begier-Krasinska B, Niklas A, et al. Comprehensive review on how platinum- and taxane-based chemotherapy of ovarian cancer affects biology of normal cells. *Cell Mol Life Sci* 2019;**76**:681−97.
54. Poruchynsky MS, Komlodi-Pasztor E, Trostel S, Wilkerson J, Regairaz M, Pommier Y, et al. Microtubule-targeting agents augment the toxicity of DNA-damaging agents by disrupting intracellular trafficking of DNA repair proteins. *Proc Natl Acad Sci U S A* 2015;**112**:1571−6.
55. Birinci H, Şen B, Sayğılı S, Ölmez E, Uluer ET, Özbilgin K. The effect of pycnogenol and paclitaxel on DNA damage in human breast cancer cell line. *Proceedings* 2017;**1**:1023.
56. Davis AJ, Chen BP, Chen DJ. DNA-PK: a dynamic enzyme in a versatile DSB repair pathway. *DNA Repair* 2014;**17**:21−9.
57. Cui X, Yu Y, Gupta S, Cho YM, Lees-Miller SP, Meek K. Autophosphorylation of DNA-dependent protein kinase regulates DNA end processing and may also alter double-strand break repair pathway choice. *Mol Cell Biol* 2005;**25**:10842−52.
58. Meek K, Douglas P, Cui X, Ding Q, Lees-Miller SP. Trans Autophosphorylation at DNA-dependent protein kinase's two major autophosphorylation site clusters facilitates end processing but not end joining. *Mol Cell Biol* 2007;**27**:3881−90.
59. Faget DV, Ren Q, Stewart SA. Unmasking senescence: context-dependent effects of SASP in cancer. *Nat Rev Cancer* 2019;**19**:439−53.
60. Boohaker RJ, Xu B. The versatile functions of ATM kinase. *Biomed J* 2014;**37**:3−9.
61. Yan HQ, Huang XB, Ke SZ, Jiang YN, Zhang YH, Wang YN, et al. Interleukin 6 augments lung cancer chemotherapeutic resistance *via* ataxia-telangiectasia mutated/NF-kappaB pathway activation. *Cancer Sci* 2014;**105**:1220−7.
62. Hsia SM, Yu CC, Shih YH, Yuanchien Chen M, Wang TH, Huang YT, et al. Isoliquiritigenin as a cause of DNA damage and inhibitor of ataxia-telangiectasia mutated expression leading to G2/M phase arrest and apoptosis in oral squamous cell carcinoma. *Head Neck* 2016;**38 Suppl 1**:E360−71.
63. Wang H, Zhang X, Teng L, Legerski RJ. DNA damage checkpoint recovery and cancer development. *Exp Cell Res* 2015;**334**:350−8.
64. Blagosklonny MV. Cell cycle arrest is not senescence. *Aging* 2011;**3**:94−101.
65. d'Adda di Fagagna F. Living on a break: cellular senescence as a DNA-damage response. *Nat Rev Cancer* 2008;**8**:512−22.
66. Gewirtz DA, Holt SE, Elmore LW. Accelerated senescence: an emerging role in tumor cell response to chemotherapy and radiation. *Biochem Pharmacol* 2008;**76**:947−57.